Orientation and Relaxation of Polymer–Clay Solutions Studied by Rheology and Small-Angle Neutron Scattering

MATTHEW M. MALWITZ,[1] PAUL D. BUTLER,[2] LIONEL PORCAR,[3] DREW P. ANGELETTE,[1] GUDRUN SCHMIDT[1]

[1]Department of Chemistry, Louisiana State University, Baton Rouge, Louisiana, 70803

[2]Oak Ridge National Laboratory, Oak Ridge, Tennessee 37831

[3]National Institute of Standards and Technology, Gaithersburg, Maryland 20899-8543

Received 4 February 2004; revised 20 March 2004; accepted 20 March 2004
DOI: 10.1002/polb.20175
Published online in Wiley InterScience (www.interscience.wiley.com).

ABSTRACT: The influence of shear on viscoelastic solutions of poly(ethylene oxide) (PEO) and clay [montmorillonite, i.e., Cloisite NA+ (CNA)] was investigated with rheology and small-angle neutron scattering (SANS). The steady-state viscosity and SANS were used to measure the shear-induced orientation and relaxation of the polymer and clay platelets. Anisotropic scattering patterns developed at much lower shear rates than in pure clay solutions. The scattering anisotropy saturated at low shear rates, and the CNA clay platelets aligned with the flow, with the surface normal parallel to the gradient direction. The cessation of shear led to partial and slow randomization of the CNA platelets, whereas extremely fast relaxation was observed for laponite (LRD) platelets. These PEO–CNA networklike solutions were compared with previously reported PEO–LRD networks, and the differences and similarities, with respect to the shear orientation, relaxation, and polymer–clay interactions, were examined. © 2004 Wiley Periodicals, Inc. J Polym Sci Part B: Polym Phys 42: 3102–3112, 2004
Keywords: clay; poly(ethylene oxide) (PEO); shear; small-angle neutron scattering (SANS); solution; relaxation

INTRODUCTION

The colloidal and rheological properties of polymer–clay nanocomposites gels and solutions[1] have received considerable attention in the literature, and good reviews are available.[2–4] Platelet ordering at the nanometer length scale is a challenging and active area of research in materials science. Nanoclay materials offer unique mechanical,[5,6] electrical,[7] optical,[7,8] and thermal properties,[5,9–14] which are the result of size quantization effects as well as the high number of surface atoms and subsequent special interface states. Property enhancements are induced by the physical presence of the nanoparticles and by the interaction of the polymer with the particles and the state of dispersion.[2,5,15,16] The developed approaches range from the manipulation of individual particles to the exploitation of self-assembly in colloids.[17,18] The large aspect ratio of platelets promotes a supramolecular organization similar to that of other mesoscopic systems, such as liquid-crystalline polymers,[19–22] surfactants,[23] and block copolymers.[24,25] Previous studies have considered the influence of nanoparticles on the structure and rheology of lamellar phases. A transition from a liquid-crystalline hexagonal phase to a lamellar phase has been observed in aqueous

Correspondence to: G. Schmidt (E-mail: gudrun@lsu.edu)
Journal of Polymer Science: Part B: Polymer Physics, Vol. 42, 3102–3112 (2004)

mixtures of a Pluronic-type block copolymer and clay. The formation of the lamellar phase is rationalized by the entropically favored packing of clay discs.[26] A recent small-angle neutron scattering (SANS) study described the adsorption of poly(ethylene oxide) (PEO) polymer chains to laponite (LRD) clay platelets at low polymer and clay concentrations (total concentration $< 5\%$).[27,28] The gelation of the clay was prevented or extremely retarded; this depended on the polymer weight and the polymer and clay concentrations. For low concentrations, the SANS contributions from bulk and adsorbed polymer chains could be separated with contrast variation methods.[27,28] Although these results were not sensitive to the shape of the polymer concentration profile, other research groups have used neutron diffraction to address the interlayer and ordered structure around each clay platelet as well as the mechanism of bridging flocculation.[29,30]

Below the threshold for the complete saturation of the clay particles by the polymer, shake gels can be generated with the consistency of a half-cooled gelatin dessert. These suspensions undergo a dramatic shear thickening when subjected to vigorous shaking.[31] Our work uses polymer–clay systems at higher concentrations and higher polymer molecular weights. In previous work, we have found the polymer chains to be entangled and to be in a dynamic adsorption–desorption equilibrium with the clay particles, forming permanent networks[32–34] that are highly elastic and behave more like soft chewing gum than gelatin. Individual polymer chains can physically absorb to several particles, and this results in strong bridging effects. In this case, SANS contrast matching methods cannot distinguish between the intensity contributions of network-active PEO, adsorbed PEO (just adsorbed, not necessarily network-active), and excess PEO (the PEO that is not attached to the clay because the clay surface is already covered) inside the network.[32–34] Despite this large body of work, polymer–clay interactions remain complex and poorly understood phenomena requiring much more investigation.

Small-angle neutron or X-ray scattering is a powerful technique for characterizing the structure and provides a measure of nanoparticle orientation under shear.[19,20,22] Scattering from an anisotropic distribution of platelets directly leads to an anisotropic scattering pattern. A two-dimensional (2D) object can align under shear along three primary directions, which are often called the *a*, *b*, and *c* orientations in the literature.[23] In the perpendicular, or *a*, orientation, the surface normals align parallel to the vorticity direction so that the particles lie in the shear gradient plane. In the transverse, or *b*, orientation, the surface normals align parallel to the shear direction so that the particles lie in the vorticity shear gradient plane. Finally, in the parallel, or *c*, direction, the surface normals align parallel to the shear gradient direction, and the particles lie in the vorticity plane.

The expected response of flat objects in a flow field is to align in the *c* orientation, and this has been seen in a number of systems of clay platelets in polymer matrices and solutions. Some of these systems have been nicely described by earlier studies on nylon-based nanocomposites reviewed by Krishnamoorti and Vaia.[3,5] Recent studies by Lele et al.[35] with *in situ* X-ray diffraction experiments have provided direct evidence for rheology–microstructure linkages in polypropylene-based nanocomposites.

Recently, we reported an unexpected case of *a* orientation for aqueous solutions of synthetic LRD clay and PEO.[34] SANS for samples in D_2O measured the shear-induced orientation of the polymer and platelets. SANS for samples with the solvent contrast matched to the clay detected the orientation of the polymer alone. When a shear field was applied, the clay particles oriented first. With increasing shear, the polymer chains started to stretch and began to contribute to the anisotropy as well. As the shear distorted and ruptured the transient gel, coupling between the composition and shear stress led to the formation of macrodomains. We have proposed that the clay orients in response to a biaxial stress arising from shear and elastic forces.[36]

A recent transmission electron microscopy (TEM) analysis by Okamoto at al.[37] has revealed a house-of-cards structure in polypropylene–clay nanocomposites subjected to elongational flow. Strong strain-induced hardening and rheopexy features at higher deformation originated from the perpendicular alignment of the silicate to the stretching direction (*b* orientation). Although TEM is not an *in situ* technique, it did reveal the difference in the clay orientation caused by shear flow versus elongational flow. Similar to the polymer–clay solutions discussed by us before,[32,33] Okamoto's nanocomposites had strong interactions between the polymer matrix and the silicate layers.

The goal of this study is to probe microscopic and nanoscopic changes in PEO–Cloisite NA+

Table 1. PEO–Clay Solution Characteristics

Sample	Mass Fraction[a] Clay (%)	PEO (%)	PEO M_w	Power Law
PEO5–CNA-6	3	5	600,000	−0.03
PEO5–CNA-10	3	5	1,000,000	−0.03
PEO5–CNA-50	3	5	5,000,000	−0.30
PEO5–LRD-10	3	5	1,000,000	−0.70
PEO2–LRD-10	3	2	1,000,000	−0.60

[a] Relative mass error <1%.

(CNA) solutions under shear. The combination of rheology and SANS provides a more complete physical picture of the shear response and relaxation behavior of these suspensions. We compare this work on PEO–CNA networklike solutions to previously reported PEO–LRD networks and focus on the differences and similarities in the shear orientation as well as the polymer–clay interactions.

EXPERIMENTAL

We prepared viscoelastic solutions of a natural smectite clay, montmorillonite (CNA, Southern Clay Products),[38] and PEO [Polysciences, Inc.; weight-average molecular weight (M_w) = 5×10^6 g/mol, weight-average molecular weight/number-average molecular weight ≈ 1.5, and radius of gyration (R_g) ≈ 200 nm in H_2O].[39] [According to ISO 31-8, the term *molecular mass* has been replaced by *relative molecular mass* (M_r). Thus, if this nomenclature and notation were to be followed, one would write M_rw, instead of the historically conventional M_w, for the mass-average molecular weight, and it would be called the *mass-average relative molecular mass*. The conventional notation, rather than the ISO notation, has been employed for this publication.]. All the CNA results reported here are for a solution containing mass fractions of 3% CNA and 5% PEO at the ambient temperature. The reference LRD samples contained 3% LRD and 2 or 5% PEO (Table 1).

The CNA clay produced an opaque suspension of predominantly exfoliated platelets [no peaks at high scattering vector (**q**) values in SANS][40] that ranged in size from 700 to 1500 Å across and were about 10 Å thick (according to atomic force microscopy).[38] The quiescent or equilibrium structure was that of a homogeneous solution with a nearly ideal polymer and clay dispersion and good adhesion between the polymer and clay. Because of the relatively high polymer and clay concentrations, we expected randomly oriented domains of oriented polymer-covered clay particles to be present. Both the pH and ionic strength of the solutions were controlled by the addition of 3.34×10^{-4} mol/L NaOH (for a pH of ca. 10) and 3.5×10^{-3} mol/L NaCl, respectively. The sample preparation was reduced to 3 weeks when the samples were mixed/sheared and centrifuged daily. Simply dissolving the polymer and the clay in water was not sufficient to completely exfoliate our samples: extensive mixing and shear were necessary to guarantee the reproducibility of the rheological experiments. All the CNA–PEO solutions used in this study were exfoliated, homogeneous, and stable for more than half a year.

Rheological experiments were performed on a Rheometrics Scientific ARES rheometer (transducer range = 0.2–2000 g cm) with either a parallel-plate (38-mm diameter and 1–2-mm gap) or Couette-type geometry. The Couette cell had a 2.0-mm gap between the cup and bob and an approximate volume of 8 mL. The shear rate dependence of the viscosity (Fig. 1) was obtained with individual, time-dependent, constant-rate experiments. Once the samples equilibrated after the cessation of shear, another time-dependent, constant-rate experiment was performed. Constant shear rates were applied for about 200 s at low shear rates ($d\gamma/dt < 5\ s^{-1}$) and for about 100 s at higher shear rates ($d\gamma/dt > 5\ s^{-1}$). These intervals were sufficient to reach a steady state, as

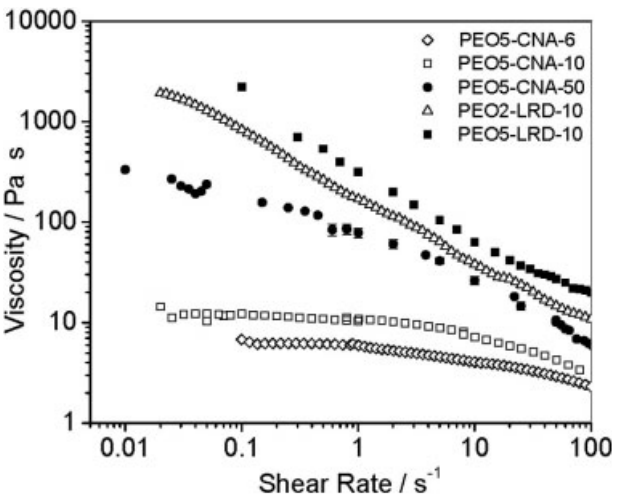

Figure 1. Steady-state viscosities of several polymer–clay solutions as a function of the shear rate.

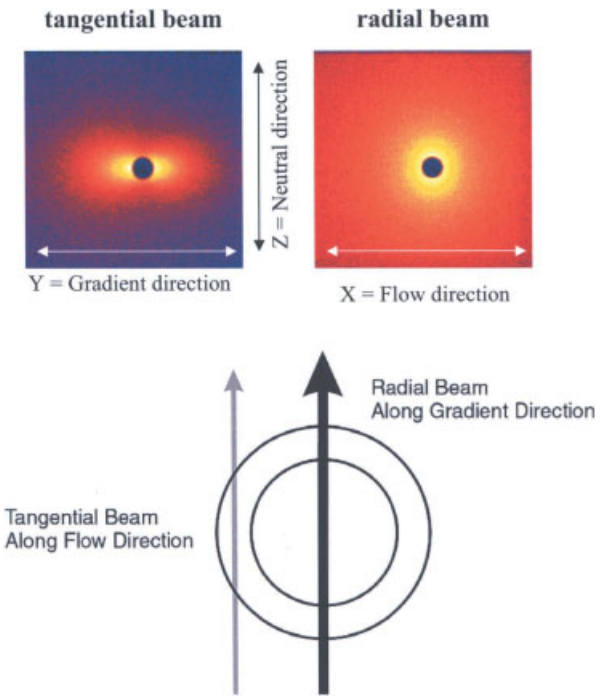

Figure 2. 2D SANS profiles (raw data) of PEO5–CNA-50 solutions obtained with the radial beam (x–z plane observed; right) and the tangential beam (y–z plane observed; left) at a shear rate of 70 s^{-1}. The anisotropy in the gradient direction is slightly influenced by reflections due to the empty Couette shear cell in the tangential beam configuration. The two profiles do not have the same scaling. The bottom figure is a top view of the Couette cell. [Color figure can be viewed in the online issue, which is available at www.interscience.wiley.com.]

determined from the time-dependent viscosity measurements. Duplicate measurements with a new sample showed the reproducibility of steady-state values within a relative error of about 7%.

SANS measurements were performed on the 30-m NG7 SANS instrument at the Center for Neutron Research of the National Institute of Standards and Technology.[41] SANS spectra were recorded simultaneously, the samples being sheared at a constant shear rate. The shear cell had a Couette-type geometry (as described previously)[42,43] with an inner diameter of 60 mm and a gap of either 0.5 or 1 mm for a total path length of either 1 or 2 mm through the sample. To study the three-dimensional (3D) clay orientation, we carried out SANS measurements with two configurations of the sample with respect to the beam (Fig. 2). In the standard configuration, called *radial beam geometry*, the incident beam was parallel to the shear gradient and traversed the center of the annular cell. In the second configuration, called the *tangential beam geometry*, the incident beam was parallel to the flow direction and tangential to the cell annulus (Fig. 2). Sample-to-detector distances of 11.2 and 1.5 m, with an incident wavelength of $\lambda = 9$ Å, were used to give a total $\mathbf{q}$ range of $0.003\ \text{Å}^{-1} < \mathbf{q} < 0.2\ \text{Å}^{-1}$. $\mathbf{q}$ is defined as $\mathbf{q} = 4\pi/\lambda \sin(\theta)$, where 2θ is the scattering angle. The scattered intensities were corrected for background and parasitic scattering.[44]

RESULTS AND DISCUSSION

Our current understanding of the previous rheology and present SANS results is that the polymer chains are in a dynamic adsorption–desorption equilibrium with the clay particles and thus form a network.[33,45] When clay particles strongly absorb to the surrounding polymer chains, the polymer does not provide a continuum medium for particle support any more. Individual polymer chains can physically absorb to several clay particles, and this results in strong bridging effects. All polymer–clay solutions (Table 1) consist of a network between clay platelets and PEO chains, with the polymer chains crosslinked between the platelets.

The steady-state values of the viscosity for two reference PEO–LRD solutions (PEO $M_w = 10^6$ g/mol) and three PEO–CNA solutions (PEO M_w = 300,000, 10^6, or 5×10^6 g/mol) are shown in Figure 1. All CNA solutions have the same polymer (5%) and clay (3%) concentrations and show shear thinning. The two reference PEO–LRD solutions contain 2 or 5% PEO and 3% LRD clay each (Table 1). At low shear rates, a power-law exponent [$m = -0.03$, viscosity = $(d\gamma/dt)^m$] can be obtained for PEO5–CNA-10 ($M_w = 1 \times 10^6$ g/mol, 5% PEO), and a change in the slope and curvature can be observed at $d\gamma/dt > 3\ s^{-1}$, whereas a reference PEO5–LRD-10 solution ($M_w = 1 \times 10^6$ g/mol, 5% PEO) previously studied by us[33] had higher viscosity and m values [$m = -0.7$, viscosity = $(d\gamma/dt)^m$].

As Figure 1 shows, for similar concentrations of the polymer and clay and a given polymer molecular weight, the viscosities of the solutions with larger clay platelets (CNA) are much lower than those of the LRD solutions with smaller clay platelets, indicating weaker interactions. Thus, it seems that polymer–clay interactions become stronger as the particle size is reduced. PEO–LRD (30-nm-diameter particles) solutions (Table 1) do not flow when a vial containing the solution

is turned upside down, whereas almost all PEO–montmorillonite solutions (100-nm-diameter particles) except PEO5–CNA-5 and comparable PEO–kaolitite solutions (micrometer-size-diameter particles) do flow. However, there are additional parameters, such as the polydispersity, surface effects, and chemistry, that may contribute to enhanced interactions. Nonetheless, this suggests that nanoscale interactions are essential for the enhancement of rheological properties at these relatively low particle concentrations.

As the polymer M_w (at a fixed polymer concentration) increases, so does the viscosity of the PEO–CNA solutions. This might be expected because of the longer and more entangled chains. However, in addition to entanglement effects, the longer individual polymer chains contain more adsorption points (crosslinks), which result in stronger bridging effects and thus also enhanced viscosity. Given the effect of pure entanglements evidenced by the rheology of a pure PEO solution described in the literature,[46] with viscosities an order of magnitude below what is observed in these polymer–clay mixtures, it is reasonable to assume that the polymer molecular weight strongly influences the density and strength of the polymer–clay bridges.

The PEO5–CNA-50 samples were shear-oriented while being loaded into the SANS shear cell, as shown by the anisotropic SANS patterns observed at rest.[47] Shear is necessary to reorient clay platelets in one direction. Steady-state viscosity experiments showed reproducible results when we switched from low to high or high to low shear rates, demonstrating that although preshearing affects start-up viscosities, it has no influence on steady-state values. All SANS data were obtained from samples in the steady-state regime. When clay particles and polymer chains are aligned in a flow field (real space), the resultant scattered intensity distribution (reciprocal space) also becomes anisotropic. The resultant anisotropy will manifest itself as an anisotropic pattern on a 2D SANS multidetector oriented parallel to the plane of anisotropy.

Representative SANS results obtained from polymer–clay solutions in the radial and tangential beam configurations are shown in Figures 2 and 3. All radial SANS patterns show isotropic intensity distributions [e.g., Fig. 2(b)], whereas all tangential SANS patterns show anisotropy parallel to the gradient axis of the flow field [Fig. 2(a)]. As shown in Figure 3, the intensities in the radial and tangential configurations do not change significantly within the measured, major shear-thinning (Fig. 1) range of shear rates (0.5–90 s^{-1}), indicating that the orientation of the PEO–CNA system as detected by SANS occurs at shear rates below about 0.5 s^{-1}. The shear thinning then must come from some other mechanism than the usual orientational effect and must instead reflect changes in more subtle polymer–clay interactions with shear. This is similar to a later discussion on relaxation times in the PEO–LRD system and nicely demonstrates the complementarities of the techniques. In any event, this PEO–CNA alignment saturates at a much lower point than that observed with the PEO–LRD systems, the alignment of which did not saturate until above 90 s^{-1}.[32–34] Thus, the data indicate that a very low flow is strong enough to orient this polymer–clay system.[32–34]

The form factor for randomly oriented discs is well known to have a $\mathbf{q}^{-2}$ dependence, as does the form factor for an unperturbed Gaussian coil, for example.[48] Thus, a plot of the logarithm of the intensity (I) versus log $\mathbf{q}$ from a system of randomly oriented, noninteracting thin disks, such as clay platelets, would be expected to have a slope of -2 over a wide $\mathbf{q}$ range, as observed by many other research groups.[49–51] For the $\mathbf{q}$ range shown in Figure 3(a) [radial beam, radial averaging of $I(\mathbf{q})$ vs $\mathbf{q}$], we note that $I(\mathbf{q})$ scales with $\mathbf{q}^{-1.6}$ (high $\mathbf{q}$) and $\mathbf{q}^{-2.8}$ (low $\mathbf{q}$). In our case, the deviations from $\mathbf{q}^{-2}$ are probably due to contributions from the scattering of polymer chains, especially at high $\mathbf{q}$ values, from the clay polydispersity, possible clustering, and clay orientation. Hanley et al.[50] attributed deviations from $\mathbf{q}^{-2}$ toward $\mathbf{q}^{-3}$ to clustering and polydispersity in montmorillonite suspensions. In the tangential beam configuration gradient direction [y direction; Fig. 3(d)], $I(\mathbf{q})$ scales with $\mathbf{q}^{-1.9}$, and this is attributed to the disc form factor. Future experiments with contrast variation techniques and partial structure factor analyses will help to separate out the individual contributions of the clay and polymer in the mixtures.

In the radial beam configuration, perfectly shear aligned platelets in the expected c orientation would be oriented with their surface normals parallel to the neutron beam, and their projection in this plane thus ideally would be seen as 2D discs with no anisotropy, whereas in the tangential beam configuration, their surface normals would be perpendicular to the neutron beam and ideally seen edge on with the projection looking like a rigid rectangle (or a needle), and the scat-

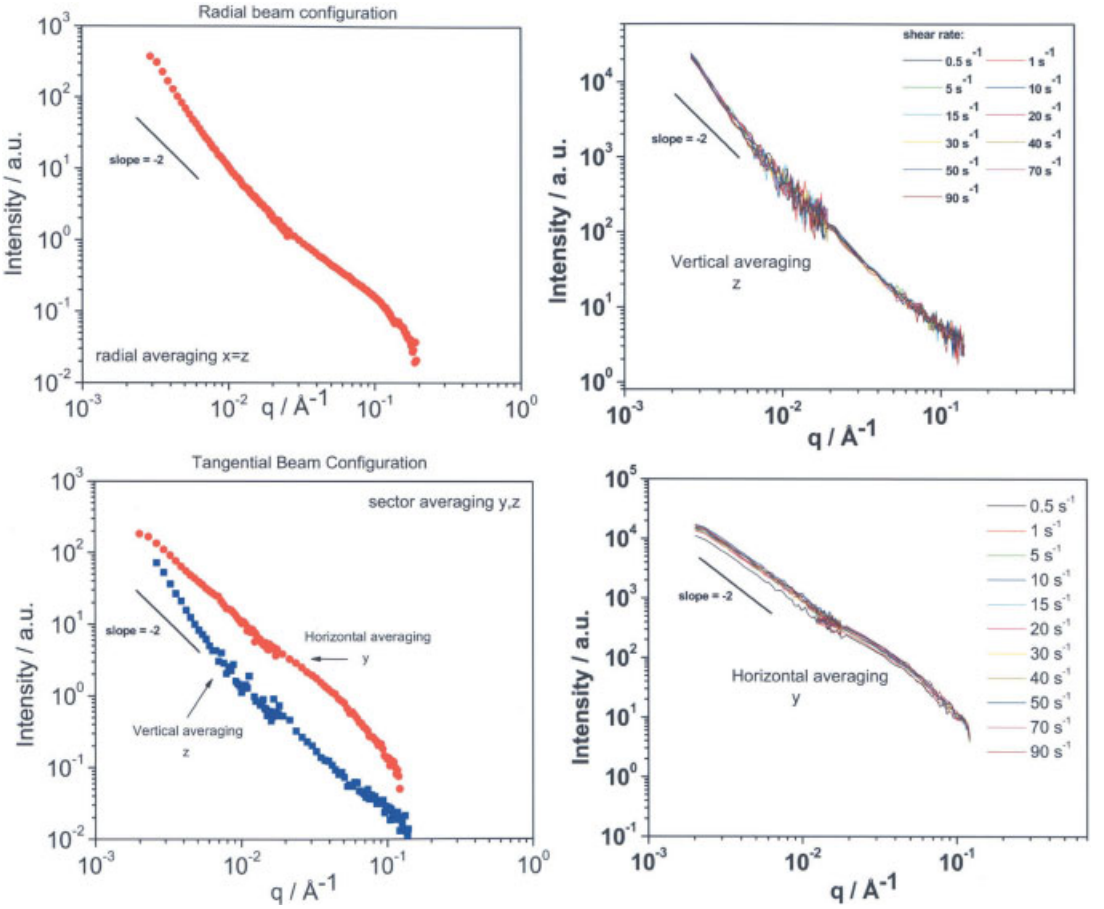

Figure 3. PEO5–CNA-50 SANS intensity averaged in 10° sectors for all three directions in space. The isotropic SANS data have been circularly averaged. In this case, the intensities in the z and x directions are the same. The SANS data have not been corrected for incoherent scattering. This may cause larger relative errors at high **q** values. Some error bars are smaller than the plotting symbols.

tering intensity would be predominantly in the horizontal (gradient) direction. The orientation of the platelets in the a orientation would lead to anisotropy in both the tangential and radial configurations. Thus, in this case, the small required shear field appears to align the platelets in the flow direction in the expected c orientation rather than the a direction observed for PEO–LRD (Fig. 4). These orientations were also observed in lamellar liquid-crystalline phases,[52,53] block copolymer solutions, and melts.[54–58]

The orientational alignment of the platelets is a competition between (1) flow alignment and (2) orientational and configurational relaxation. At a given shear rate, the relaxation processes must be hindered by a coupling between the polymer and clay. With arguments similar to those of Ramsay and Lindner[49] and Hayter and Penfold,[59] competing effects can be characterized by the dimensionless Weissenberg parameter ($\Gamma = g\tau$, where g is the shear rate and τ is the relaxation time). Full alignment will occur for $\Gamma \gg 1$. In this study, the alignment of the PEO–CNA system starts at shear rates $\ll 0.5\ s^{-1}$, whereas the PEO–LRD systems containing smaller LRD particles studied previously[32] begin to align at shear rates of about $5\ s^{-1}$. This corresponds to characteristic relaxation times of $\tau \gg 2$ s for the PEO–CNA system and $\tau \approx 0.05$ s for PEO–LRD.[32] Although Hayter and Penfold studied micellar solutions 20 years ago, our polymer–clay solutions and gels pose different challenges because the polymer and clay orientational relaxation times can be very different. Future contrast matching studies should be able to help separate these components. If the shear becomes large enough to disrupt the clay–

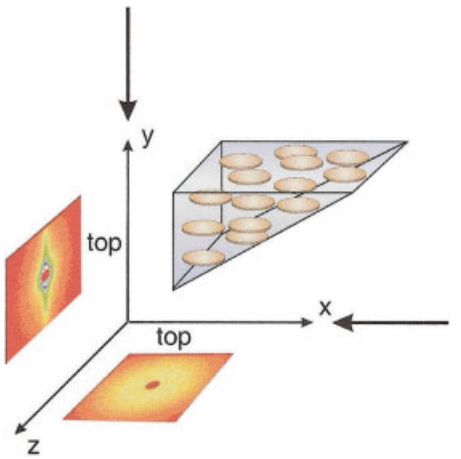

Figure 4. Model for the real space orientation of CNA clay platelets and corresponding reciprocal space SANS patterns (x = flow direction, y = gradient or velocity direction, and z = vorticity or neutral direction). As the CNA platelets align with the surface normal along the velocity direction, we can observe an isotropic radial SANS pattern (beam in y) and a horizontal streak in the tangential SANS pattern (beam in x). An imperfect orientation of platelets is assumed. [Color figure can be viewed in the online issue, which is available at www.interscience.wiley.com.]

polymer interactions, it is possible for phase separation to occur. Effects similar to shear banding have been observed within rheology and microscopy experiments for both PEO–LRD and PEO–CNA solutions at very high shear rates and over long shear times. The relaxation of PEO–CNA after the cessation of shear is slow, as would be expected from the very low shear rates for alignment, and on the timescale of the experiments (>2 h) is incomplete, with the anisotropic peaks in the SANS patterns (discussed later) relaxing to only about half their original height in 70 min.

There are a variety of ways of characterizing the anisotropy in sheared SANS data. Dadmun and Han,[20] for example, characterized anisotropy in scattering patterns in terms of peak heights and widths of azimuthal intensity scans. They used the peak height to characterize changes in the molecular orientation. With this procedure, the azimuthal trace of PEO–CNA data was fit with a Lorenzian curve, and the width and peak height were plotted as functions of the time that elapsed after the cessation of shear. Data obtained from azimuthal averaging at (1) $\mathbf{q} \approx 0.07$ Å^{-1} and $d \approx 90$ Å (d = characteristic dimension $d = 2\pi/q$) are shown in Figure 6(a), and data obtained at (2) $\mathbf{q} \approx 0.007$ Å^{-1} and $d \approx 900$ Å are shown in Figure 6(b). The SANS relaxations for 1 and 2 indicate that after 120 min there is still some anisotropy visible. The results displayed in Figures 5 and 6 show that the PEO–CNA samples relax back to a much lower degree of orientation but do not randomize completely as PEO–LRD solutions do.

The Hermans orientation function (f) or nematic order parameter can be used to quantitatively assess the degree of orientation at any point in the relaxation process as follows:[60,61]

$$f = \frac{3\langle \cos^2 \phi \rangle - 1}{2}$$

$$\text{and} \qquad \langle \cos^2 \phi \rangle = \frac{\int_0^{\pi/2} I \cos^2\phi \sin\phi \, d\phi}{\int_0^{\pi/2} I \sin\phi \, d\phi} \qquad (1)$$

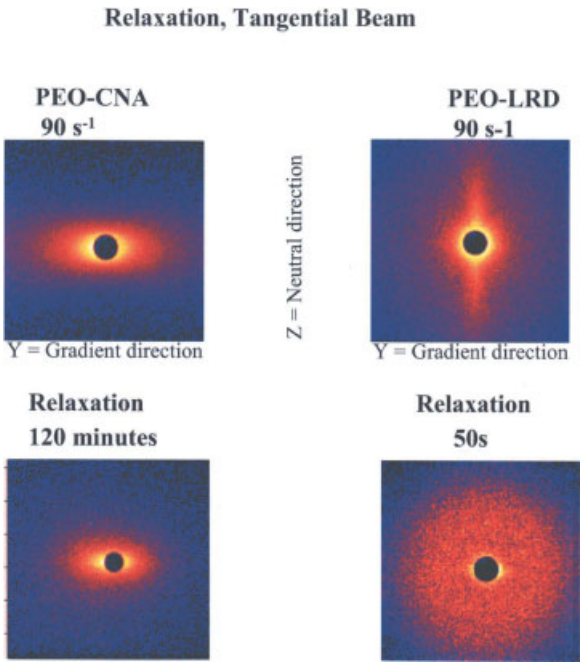

Figure 5. Tangential SANS data for PEO5–CNA-50 and PEO2–LRD-10 at a shear rate of 90 s^{-1} and the relaxation of the SANS intensity after the cessation of shear (similar **q** range). [Color figure can be viewed in the online issue, which is available at www.interscience.wiley.com.]

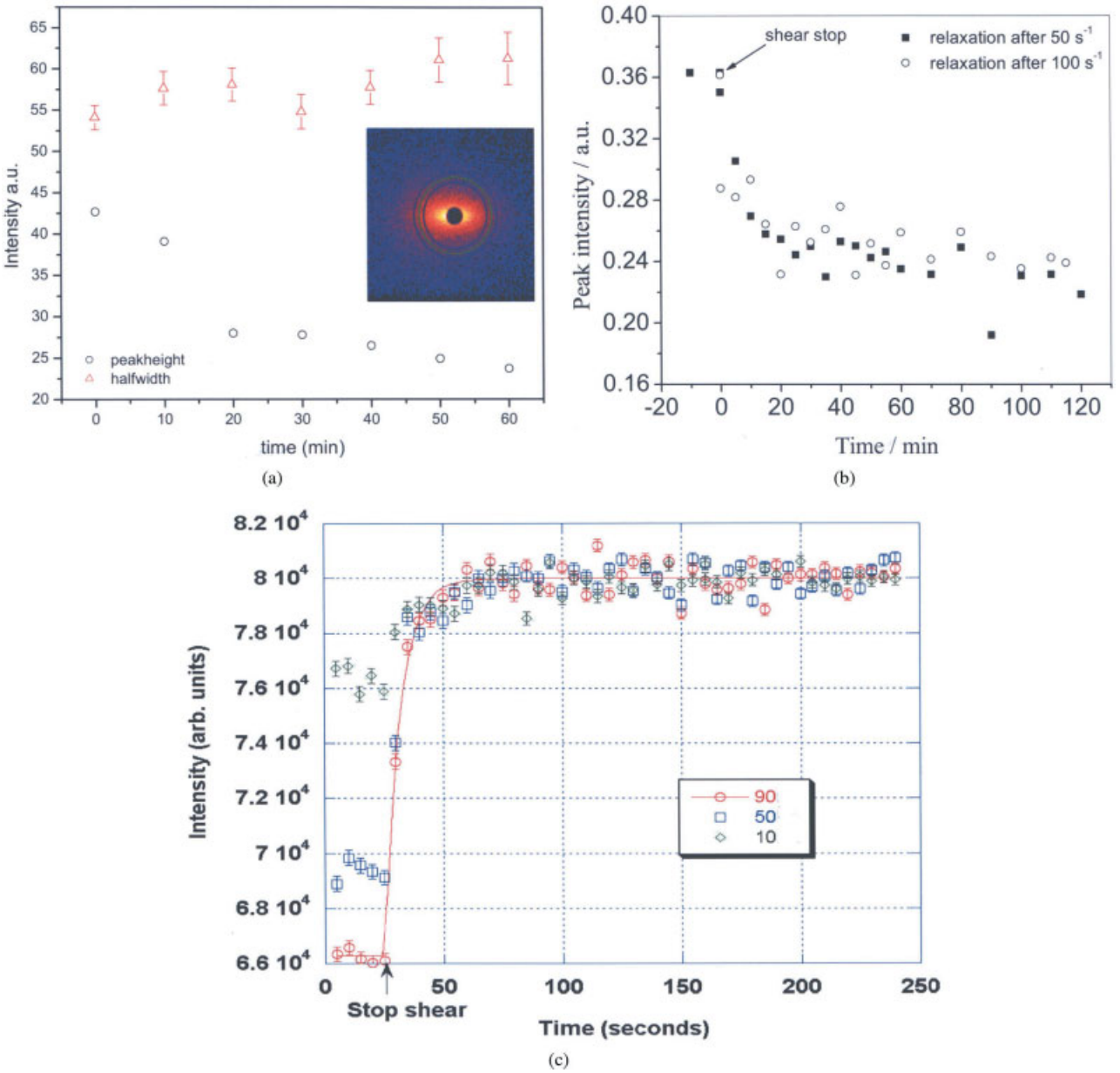

Figure 6. (a,b) PEO–CNA relaxation of anisotropic SANS patterns (tangential beam configuration): peak height and half-width of the azimuthal intensity distribution (from a Lorenzian fit) as functions of the elapsed time after the cessation of shear, with azimuthal averaging at (a) $\mathbf{q} \approx 0.07$ Å^{-1} and $d \approx 90$ Å (the insert shows an SANS pattern with an azimuthal ring used to calculate the anisotropy) and (b) $\mathbf{q} \approx 0.007$ Å^{-1} and $d \approx 900$ Å. (c) PEO–LRD relaxation with time-slicing procedures: total SANS intensity (y axis) versus time after the cessation of shear (time slicing procedure as described in ref. 63). Shear rates used before shear stop are: 90 s^{-1} (circle), 50 s^{-1} (square), and 10 s^{-1} (diamond). [Color figure can be viewed in the online issue, which is available at www.interscience.wiley.com.]

where $\langle \cos^2 \phi \rangle$ is the average cosine squared weighted by I as a function of the radial angle (ϕ).[62] Thus, f varies between $f = 1$, corresponding to a perfect orientation, and $f = 0$, corresponding to a random orientation. With azimuthally averaged data for $\mathbf{q} = 0.07$ Å^{-1} (SANS configuration = 1 m), the PEO–CNA solution yields $f = 0.85$ at a shear rate of 90 s^{-1}; this decreases to $f = 0.74$

within 70 min after the cessation of shear, indicating that complete randomization ($f = 0$) would probably take weeks and is thus experimentally inaccessible to SANS.

Anisotropic SANS data from PEO–LRD solutions, on the other hand, relax to completely isotropic patterns within 50 s (Figs. 5 and 6), and this makes it hard to quantify the relaxation time. To provide some measure of this fast relaxation, a time-slicing procedure[63] was used to obtain better time resolution. To maximize the signal from this relatively time intensive and inherently low-intensity measurement, we used a PEO2–LRD-10 solution to eliminate the large background signal from unaligned excess PEO, whereas the change in the alignment with time was quantified by the plotting of the total SANS intensity versus the time in Figure 6(c).[64] These data indicate that, regardless of the initial degree of alignment, the time constant for orientational relaxations is approximately 7 s. However, better time resolution is clearly needed to obtain an accurate value with the PEO5–LRD-10 solution. Despite this very rapid orientational relaxation in PEO–LRD solutions, stress–relaxation measurements show that full relaxation requires much longer times (ca. 30 min). As mentioned earlier, this is another example of the complementarity of the two techniques (SANS and rheology). Nonetheless, the relaxation behavior after the cessation of shear is currently still poorly understood.

To understand the PEO–CNA results, we propose that as the polymer chains adsorb to the clay particles, they build a connected 3D network, much as we proposed for a similar networklike polymer–clay system containing much smaller platelets (30-nm-diameter LRD).[32–34] The polymer chains are envisioned to be entangled and in adsorption–desorption equilibrium with the clay particles, exhibiting characteristics of soft, reversible physical crosslinkers. Several studies besides our own work have shown that PEO polymer chains are very silicatophilic, and this makes our model reasonable.[65–67] Further evidence for such connectivity is the fact that long, strongly birefringent fibers (up to 8 m long and 2 μm in diameter) can be manually drawn from CNA–PEO and PEO–LRD solutions; this is not possible with either pure clay or a pure percolated polymer solution on its own. Polymer molecular weights of 10^6 g/mol (R_g = 100 nm in aqueous solutions) or higher are necessary to produce these fibers. A pure reference PEO solution with up to 2% ($M_w = 10^6$ g/mol) at the same pH and salt concentration has been found to produce no anisotropic SANS patterns at shear rates of up to about 100 s^{-1}.[32,33] Pure reference PEO solutions discussed in the literature behave like shear-thinning viscous fluids with a Newtonian plateau at low shear rates.[36] It is not possible to completely dissolve larger amounts (5%) of high-molecular-weight PEO in water without phase-separation effects and aggregation. The polymer–clay absorption and interactions, however, increase the solubility of polymer in water, stabilizing our solutions. Finally, as another indication of a strong polymer–clay network, we note that our PEO–CNA and PEO–LRD samples could not be diluted without flocculation and macroscopic phase separation.

The two PEO–clay systems clearly have very different dynamics. Under comparable conditions (similar polymer concentration, pH, and salt), large CNA clay platelets (diameter = 100 nm) align much more readily under flow than smaller LRD clay platelets (diameter = 30 nm)[32–34] and relax from that alignment much more slowly as well. This is a new and unexpected result that we need to explain with further rheological studies. The size of the clay may thus play an important role in relaxation processes, and the nanoscale interactions influence the macroscopic behavior. Finally, the interactions between the polymer and clay may be somewhat different because of the nature of the clay. These interactions and the kinetics of the adsorption–desorption equilibrium of polymer chains to the clay surfaces influence the strength of the network. The dispersion and stabilization of clay platelets in an aqueous polymer solution occur because of hydrogen bonding as well as strong dipole interactions between PEO chains and charged clay surfaces. Polymer–clay interactions depend on many parameters, such as the polymer and clay concentration, clay chemistry, clay size distribution, surface treatment, solvent type, pH, and salt.

Our unexpected results pose many open questions, and more experiments are necessary for a quantitative evaluation. Planned SANS measurements may help us to determine the thickness and density of the polymer–clay interfacial region, the average number of contacts per chain and per particle for the different sizes of the clay particles, and the different polymer molecular weights. Once we have obtained this information, we can determine how the polymer–clay interactions influence the macroscopic behavior. Planned dynamic testing will lead to further elucidation of the rheological behavior for a better understand-

ing of the viscoelasticity-, relaxation-, and interaction-based phenomena.[68] This information will be important for better controlling the fluidity of nanocomposite systems and thus changing their mechanical and electronic properties. Further experiments are required to fully and quantitatively characterize the polymer–clay interactions in these fascinating and extremely complex systems.

The authors acknowledge the financial support of a National Science Foundation CAREER award (DMR 0348884), a Louisiana Board of Regents grant [LEQSF (2002-05)-RD-A-09], and the National Science Foundation IGERT program at Louisiana State University. They also acknowledge the support of the National Institute of Standards and Technology and the National Science Foundation, through agreement number DMR 9986442, in providing the neutron research facilities used in this work. The identification of any commercial or trade name does not imply endorsement or recommendation by the National Institute of Standards and Technology. Oak Ridge National Laboratory is managed for the U.S. Department of Energy by UT-Batelle LLC under contract number DE-AC0500OR22725. Finally, the authors thank the reviewers for their helpful comments.

REFERENCES AND NOTES

1. Aubry, T.; Bossard, F.; Moan, M. Langmuir 2002, 18, 155–159.
2. Luckham, P. F.; Rossi, S. Adv Colloid Interface Sci 1999, 82, 43–92.
3. Krishnamoorti, R.; Yurekli, K. Curr Opin Colloid Interface Sci 2001, 6, 464–470.
4. Vaia, R. A.; Gianellis, E. P. MRS Bull 2001, 62, 394–401.
5. Krishnamoorti, R.; Vaia, R. A. Polymer Nanocomposites; American Chemical Society: Washington, DC, 2002; Vol. 804.
6. Kojima, Y.; Usuki, A.; Kawasumi, M.; Okada, A.; Fukushima, Y.; Kurauchi, T.; Kamigaito, O. J Mater Res 1993, 8, 1185–1189.
7. Chapman, R.; Mulvaney, P. Chem Phys Lett 2001, 349, 358–362.
8. Wilson, O.; Wilson, G. J.; Mulvaney, P. Adv Mater 2002, 14, 1000.
9. Yoon, P. J.; Fornes, T. D.; Paul, D. R. Polymer 2002, 43, 6727–6741.
10. Giannelis, E. P.; Krishnamoorti, R.; Manias, E. Adv Polym Sci 1999, 138, 107–147.
11. Burnside, S. D.; Giannelis, E. P. Chem Mater 1995, 7, 1597–1600.
12. Burnside, S. D.; Giannelis, E. P. J Polym Sci Part B: Polym Phys 2000, 38, 1595–1604.
13. Lee, D. C.; Jang, L. W. J Appl Polym Sci 1998, 68, 1997–2005.
14. Gilman, J. W. Appl Clay Sci 1999, 15, 31–49.
15. Lagaly, G. Appl Clay Sci 1999, 15, 1–9.
16. Burnside, S. D.; Wang, H. C.; Giannelis, E. P. Chem Mater 1999, 11, 1055–1060.
17. Schmidt, G.; Malwitz, M. M. Curr Opin Colloid Interface Sci 2003, 8, 103–108.
18. Gabriel, J. C. P.; Camerel, F.; Lemaire, B. J.; Desvaux, H.; Davidson, P.; Batail, P. Nature 2001, 413, 504–508.
19. Hongladarom, K.; Ugaz, V. M.; Cinader, D. K.; Burghardt, W. R.; Quintana, J. P.; Hsiao, B. S.; Dadmun, M. D.; Hamilton, W. A.; Butler, P. D. Macromolecules 1996, 29, 5346–5355.
20. Dadmun, M. D.; Han, C. C. Macromolecules 1994, 27, 7522–7532.
21. Schmidt, G.; Muller, S.; Schmidt, C.; Richtering, W. Rheol Acta 1999, 38, 486–494.
22. Walker, L. M.; Wagner, N. J. Macromolecules 1996, 29, 2298–2301.
23. Butler, P. Curr Opin Colloid Interface Sci 1999, 4, 214–221.
24. Bates, F. S.; Koppi, K. A.; Tirrell, M.; Almdal, K.; Mortensen, K. Macromolecules 1994, 27, 5934–5936.
25. Schmidt, G.; Richtering, W.; Lindner, P.; Alexandridis, P. Macromolecules 1998, 31, 2293–2298.
26. Castelletto, V.; Ansari, I. A.; Hamley, I. W. Macromolecules 2003, 36, 1694–1700.
27. Lal, J.; Auvray, L. J Appl Crystallogr 2000, 33, 673–676.
28. Lal, J.; Auvray, L. Mol Cryst Liq Cryst 2001, 356, 503–515.
29. Swenson, J.; Smalley, M. V.; Hatharasinghe, H. L. M.; Fragneto, G. Langmuir 2001, 17, 3813–3818.
30. Smalley, M. V.; Hatharasinghe, H. L. M.; Osborne, I.; Swenson, J.; King, S. M. Langmuir 2001, 17, 3800–3812.
31. Zebrowski, J.; Prasad, V.; Zhang, W.; Walker, L. M.; Weitz, D. A. Colloids Surf A 2003, 213, 189–197.
32. Schmidt, G.; Nakatani, A. I.; Butler, P. D.; Han, C. C. Macromolecules 2002, 35, 4725–4732.
33. Schmidt, G.; Nakatani, A. I.; Butler, P. D.; Karim, A.; Han, C. C. Macromolecules 2000, 33, 7219–7222.
34. Schmidt, G.; Nakatani, A. I.; Han, C. C. Rheol Acta 2002, 41, 45–54.
35. Lele, A.; Mackley, M.; Galgali, G.; Ramesh, C. J Rheol 2002, 46, 1091–1110.
36. Lin-Gibson, S.; Schmidt, G.; Kim, H.; Han, C. C.; Hobbie, E. K. J Chem Phys 2003, 119, 8080–8083.
37. Okamoto, M.; Nam, P. H.; Maiti, P.; Kotaka, T.; Hasegawa, N.; Usuki, A. Nano Lett 2001, 1, 295–298.
38. The polydispersity was estimated by the supplier to be about 30%.

39. Brandup, J.; Immergut, E. H.; Grulke, E. A. Polymer Handbook; Wiley: New York, 1999.
40. Ho, D. L.; Briber, R. M.; Glinka, C. J. Chem Mater 2001, 13, 1923–1931.
41. Glinka, C. J.; Barker, J. G.; Hammouda, B.; Krueger, S.; Moyer, J. J.; Orts, W. J. J Appl Crystallogr 1998, 31, 430–445.
42. Straty, G. C.; Muzny, C. D.; Butler, B. D.; Lin, M. Y.; Slawecki, T. M.; Glinka, C. J.; Hanley, H. J. M. Phys B 1997, 241, 74–76.
43. Straty, G. C.; Muzny, C. D.; Butler, B. D.; Lin, M. Y.; Slawecki, T. M.; Glinka, C. J.; Hanley, H. J. M. Nucl Instrum Methods Phys Res Sect A 1998, 408, 511–517.
44. NG3 and NG7 30-Meter SANS Instruments Data Acquisition Manual; Cold Neutron Research Facility at the National Institute of Standards and Technology: Gaithersburg, MD, 1999.
45. Schmidt, G.; Nakatani, A. I.; Han, C. C. Rheol Acta 2002, 41, 45–54.
46. Lin-Gibson, S.; Kim, H.; Schmidt, G.; Han, C. C.; Hobbie, E. K. Journal of Colloid and Interface Science 2004, 274, 515–525.
47. Preliminary flow–birefringence experiments also support these results. Depending on the orientation and size of the domains as well as the sample history during filling, birefringence from a new sample is always slightly different and nonzero. This birefringence can be easily visualized with a microscope and crossed polarizers.
48. Guinier, A.; Fournet, G. Small Angle Scattering of X Rays; Wiley: New York, 1955.
49. Ramsay, J. D. F.; Lindner, P. J Chem Soc Faraday Trans 1993, 89, 4207–4214.
50. Hanley, H. J. M.; Muzny, C. D.; Ho, D. L.; Glinka, C. J. Langmuir 2003, 19, 5575–5580.
51. Morvan, M.; Espinat, D.; Lambard, J.; Zemb, T. Colloids Surf A 1994, 82, 193–203.
52. Diat, O.; Roux, D.; Nallet, F. J Phys IV 1993, 3, 193–204.
53. Diat, O.; Roux, D.; Nallet, F. J Phys II 1993, 3, 1427–1452.
54. Leist, H.; Maring, D.; Thurn-Albrecht, T.; Wiesner, U. J Chem Phys 1999, 110, 8225–8228.
55. Maring, D.; Wiesner, U. Macromolecules 1997, 30, 660–662.
56. Chen, Z. R.; Kornfield, J. A.; Smith, S. D.; Grothaus, J. T.; Satkowski, M. M. Science 1997, 277, 1248–1253.
57. Chen, Z. R.; Issaian, A. M.; Kornfield, J. A.; Smith, S. D.; Grothaus, J. T.; Satkowski, M. M. Macromolecules 1997, 30, 7096–7114.
58. Fredrickson, G. H.; Bates, F. S. Annu Rev Mater Sci 1996, 26, 501–550.
59. Hayter, J. B.; Penfold, J. J Phys Chem 1984, 88, 4589–4593.
60. Hermans, P. H.; Hermans, J. J.; Vermaas, D.; Weidinger, A. J. J Polym Sci 1947, 3, 393–406.
61. Hermans, P. H.; Kolloid-Zeitschrift 1941, 97, 223–228; and de Booys, J.; Herman, P. H. Kolloid-Zeitschrift 1941, 97, 229–231.
62. The vectors at 0 and 90° have between them angle ϕ.
63. Hamilton, W. A.; Butler, P. D.; Magid, L. J.; Han, Z.; Slawecki, T. M. Phys Rev E 1999, 60, R1146–R1149.
64. Although ideally we would like to limit the number of parameters being altered, this is often impossible, in large part because of the very complicated phase diagrams of these complex systems. For example, although PEO2–LRD-10 (Table 1) is the sample with the most network-active PEO, it is not possible to prepare anything exactly comparable to CNA because under similar conditions [e.g., same polymer M_w and same polymer (2%) and clay (3%) concentrations], a PEO–CNA solution or mixture will strongly phase-separate. On the other hand, PEO5–LRD-10 appears to have a considerable amount of excess PEO, the isotropic scattering signal of which provides a large background signal that is very difficult to handle here. This is not the case for PEO5–CNA-10. Thus, the choice of samples is limited by the phase diagrams and the limitations of the technique involved. However, the relaxation times for the various LRD samples are of the same order and are much faster than those of the CNA solutions. Here we are able to roughly quantify that.
65. Imperor-Clerc, M.; Davidson, P.; Davidson, A. J Am Chem Soc 2000, 122, 11925–11933.
66. Goltner-Spickermann, C. Top Curr Chem 2003, 226, 29–54.
67. Goltner-Spickermann, C. Curr Opin Colloid Interface Sci 2002, 7, 173–178.
68. Sternstein, S. S.; Zhu, A. J. Macromolecules 2002, 35, 7262–7273.